Science Bulletin 65 (2020) 791–795

Contents lists available at ScienceDirect

Science Bulletin

journal homepage: www.elsevier.com/locate/scib

Science Bulletin
www.scibull.com

Short Communication

# Solution-processed ultra-flexible C8-BTBT organic thin-film transistors with the corrected mobility over 18 $cm^2/(V\ s)$

Pengshan Xie [a,1], Tianjiao Liu [a,1], Jia Sun [a,1], Jie Jiang [a], Yongbo Yuan [a], Yongli Gao [a,b], Jianfei Zhou [c], Junliang Yang [a,*]

[a] State Key Laboratory of Powder Metallurgy, School of Physics and Electronics, Central South University, Changsha 410083, China
[b] Department of Physics and Astronomy, University of Rochester, New York, NY 14627, USA
[c] Lucky Huaguang Graphics Co., Ltd, Nanyang 473003, China

ARTICLE INFO

*Article history:*
Received 6 February 2020
Received in revised form 19 February 2020
Accepted 22 February 2020
Available online 10 March 2020



Organic thin film transistors (OTFTs) show great potential for applications in low-cost, light-weight flexible electronics. OTFTs were first reported in 1986 with polythiophene as the active layer material with a mobility of ~$10^{-5}$ $cm^2/(V\ s)$ [1]. Since then, OTFTs have shown impressive improvements in device performance parameters, e.g., mobility improved by over 4 orders of magnitude. These advances followed discoveries of new materials and improvements in device engineering, as well as in morphology and interface engineering [2–4]. Flexible OTFTs (*f*-OTFTs) as a very important electronic component in flexible electronics are attracting a great deal of attention from both academic and industrial communities. Presently, *f*-OTFTs are potentially used for electronic skin [5], flexible organic integrated circuits [6], flexible active matrix displays [7] and neuromorphic devices [8].

However, the mobility of the state-of-the-art *f*-OTFTs is commonly between 0.1 and 10 $cm^2/(V\ s)$, lower than that of crystalline silicon and metal oxide TFTs, which greatly limits their practical applications. Recently, significant effort has been made to improve the performance of *f*-OTFTs. Ji et al. [9] developed copolymer dielectrics with balanced chain packing density and surface polarity for manufacturing vacuum-evaporated pentacene *f*-OTFTs with a high mobility of 5.6 $cm^2/(V\ s)$ and a low operating voltage of about 3 V. Wang et al. [10] developed intrinsically stretchable *f*-OTFTs array with an on/off current ratio ($I_{on}/I_{off}$) as high as $10^4$ and an average mobility of 1.37 $cm^2/(V\ s)$. Wang et al. [11] applied controllable vacuum evaporation to fabricate *f*-OTFTs with organic semiconductor dinaphtho[2,3-b:2′,3′-f]thieno[3,2-b]thiophene (DNTT) with the charge mobility reaching 2.8 $cm^2/(V\ s)$. However, it is still a great challenge to produce *f*-OTFTs with mobility over 10 $cm^2/(V\ s)$ and high flexibility.

Organic semiconductor 2,7-dioctyl[1] benzothieno[3,2-b][1] benzothiophene (C8-BTBT) (Fig. S1 online) is widely used as the active layer in OTFTs and exhibits high mobilities over 10 $cm^2/(V\ s)$ on rigid substrates [12,13]. Recently, ultrathin *f*-OTFTs based on C8-BTBT thin film via a peeling-off process have reached an average mobility of 7.22 $cm^2/(V\ s)$ [14]. In order to ensure C8-BTBT *f*-OTFTs competitiveness with their inorganic counterparts and to promote commercial applications, the device fabrication should be simple, inexpensive, solution-processable, and compatible with large-area processing and high-throughput manufacturing approaches such as roll-to-roll (R2R) printing. Herein, R2R slot-die printing of large-area and uniform silver nanowires (AgNWs) onto poly(ethylene terephthalate) (PET) substrate is employed as gate electrode for constructing high-performance C8-BTBT *f*-OTFTs via solution process. The corrected highest and average mobilities of C8-BTBT *f*-OTFTs can reach over 18 and 13 $cm^2/(V\ s)$, respectively. Furthermore, the *f*-OTFTs show excellent mechanical flexibility and the corrected average mobility can retain over 10 $cm^2/(V\ s)$ even after 2000 bending cycles at a bending radius of 6 mm.

R2R coating processes are suitable for low-cost and high-output fabrication of large-scale *f*-OTFTs [15]. The AgNWs transparent conductive layer on PET substrate is fabricated via R2R slot-die coating process with the diameter of 70–100 nm (Fig. S2 online). The schematic of R2R slot-die coating process is shown in Fig. 1a, and the sheet resistance of resulted AgNWs/PET film is about 26.2 Ω/□, as shown in Fig. S3a (online). The bottom-gate/top-contact C8-BTBT *f*-OTFTs are constructed on 125-μm-thick PET substrate (Fig. 1b), in which C8-BTBT is used as the active layer, cross-linked poly(4-vinyl-phenol)-4,4′-(hexafluoroisopropylidene) diphthalic anhydride (PVP-HDA, Fig. S1 online) is the dielectric layer, and R2R slot-die coated AgNWs or a composite layer of

* Corresponding author.
*E-mail address:* junliang.yang@csu.edu.cn (J. Yang).
[1] The authors contributed equally to this work.

https://doi.org/10.1016/j.scib.2020.03.013
2095-9273/

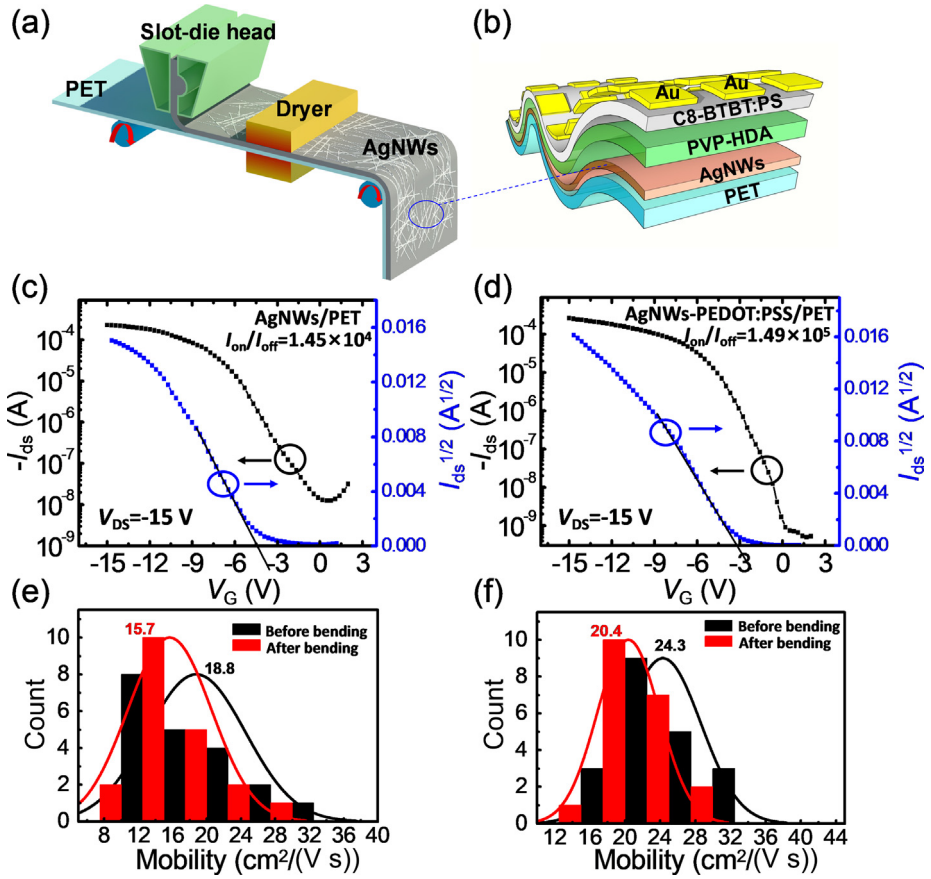


**Fig. 1.** (Color online) Solution-processed high-performance C8-BTBT *f*-OTFTs using R2R slot-die coated AgNWs as the gate electrode. (a) Schematic diagram of R2R slot-die coating AgNWs process. (b) Schematic diagram of C8-BTBT *f*-OTFTs with a bottom-gate/top-contact structure, in which the PET is covered with AgNWs or AgNWs-PEDOT:PSS used as the gate electrode. (c), (d) Typical transfer characteristics of *f*-OTFTs with AgNWs and AgNWs-PEDOT:PSS as the gate electrode, respectively. (e), (f) The statistical diagrams of mobilities based on 20 *f*-OTFTs before and after 2000 cycles bending test using AgNWs and AgNWs-PEDOT:PSS gate electrode, respectively. Black color denotes *f*-OTFTs without bending while red denotes *f*-OTFTs after 2000 cycle bending.

AgNWs and poly(3,4-ethylenedioxythiophene):polystyrene sulfonate (AgNWs-PEDOT:PSS) is used as the gate electrode. It was demonstrated that incorporating optimized 10 wt% polystyrene (PS, Fig. S1 online) into C8-BTBT is favorable for improving viscosity and retarding the crystallization of C8-BTBT during off-center spin-coating (OCSC) deposition, which facilitates the formation of highly uniform crystalline C8-BTBT semiconducting thin film [12]. Thus, C8-BTBT incorporated with 10 wt% PS deposited via OCSC process was used to process high-quality active layer. The transmission spectrum of C8-BTBT/cross-linked PVP-HDA film on AgNWs/PET exhibits that the optical transparency reaches 88% in the wavelength of 350 to 800 nm, as shown in Fig. S3b (online), and the photograph of C8-BTBT *f*-OTFT arrays in Fig. S3c (online) shows good flexibility and transparency.

The typical transfer and output curves of C8-BTBT *f*-OTFTs with AgNWs gate electrode are shown in Figs. 1c and S4a (online). The transfer curve unambiguously indicates that the C8-BTBT *f*-OTFTs exhibit high source-drain current up to 110 μA and the off-state current is about 12.5 nA at $V_G$ = 0.48 V, showing effective modulation under the gate voltage. The threshold voltage ($V_{th}$) approaches −4 V. The output curves in Fig. S4a (online) exhibit clear pinch-off and current saturation. In order to evaluate the mobility, the specific capacitance of PVP-HDA is measured with an Au/PVP-HDA/AgNWs (MIM) structure from 20 Hz to 1 MHz, as shown in Fig. S5 (online). The capacitance per unit area of PVP-HDA is measured to be around 10.5 nF/cm$^2$ at 20 Hz and is used to calculate the mobility of the devices. The field-effect mobility in the saturation regime is extracted using the relationship:

$$\mu_{sat} = \frac{2L}{W} \times \frac{I_D}{C_i \times (V_G - V_{th})^2}, \quad (1)$$

where $C_i$ is the insulator capacitance per unit area, and $W$ and $L$ are the width and length of the channel, respectively. Thus, the mobility as high as 32.9 cm$^2$/(V s) (Fig. 1c) can be achieved with an acceptable current on/off ratio ($I_{on}/I_{off}$) of 1.45 × 10$^4$.

In order to further optimize the performance of C8-BTBT *f*-OTFT devices, the PEDOT:PSS is employed for modifying the surface of AgNWs gate electrode. As compared with AgNWs gate electrode, the sheet resistance of AgNWs-PEDOT:PSS increases modestly to a value of 31.3 Ω/□ (Fig. S3a online). Meanwhile, the transparency of C8-BTBT:PS/PVP-HDA/AgNWs-PEDOT:PSS in the visible light region still exceeds 85% (Fig. S3b online). The specific capacitance of Au/PVP-HDA/AgNWs-PEDOT:PSS capacitor is measured to be 12.5 nF/cm$^2$ at 20 Hz, as shown in Fig. S5 (online). Using AgNWs-PEDOT:PSS instead of AgNWs as the gate electrode results in an improved mobility reaching 33.6 cm$^2$/(V s) (Fig. 1d), which is a little lower than that of C8-BTBT OTFTs on a rigid substrate [12]. Furthermore, the off-current is as low as 0.49 nA and the $I_{on}/I_{off}$ ratio is improved to over 10$^5$. The output curves, as shown in Fig. S4b (online), exhibit remarkable modulation capability.

At present, there are still some issues concerning the mobility calculation of OTFTs. A large number of works have demonstrated that the mobility of OTFTs is overestimated by using traditional transistor's theory since the formulas used to calculate the mobility are valid only for ideal OTFTs both in linear region and saturation region. Very recently, Choi et al. [16] described several kinds of

error calculations in detail and proposed a parameter, measurement reliability factor *r*, which can be used to quickly gauge the overall effectiveness of mobility. The *r* is given by:

$$r = \left( \frac{\sqrt{|I_D|^{max}} - \sqrt{|I_D^0|}}{|V_G|^{max}} \right)^2 \div \left( \frac{WC_i}{2L} \times \mu_{sat} \right)_{initial}, \quad (2)$$

where $|I_D|^{max}$ is the experimental maximum source–drain current reached at the maximum gate voltage $|V_G|^{max}$. $I_D^0$ represents the source-drain current when $V_G$ is equal to 0. According to this method, the mobility of devices is recalculated by using $\mu_{initial} \times r$. The transfer characteristic curves of our devices can be considered similar to one of the overestimated cases, i.e., the slight "double-slop" phenomena [16,17]. The two typical characteristic curves of *f*-OTFTs based on AgNWs and AgNWs-PEDOT:PSS gate electrodes are shown in Fig. S6a and c (online). The mobility based on the slope of transfer curve at the large $V_G$ above the "knee" is calculated, where $\mu_1$ means the original calculation results and $\mu_2$ means the calculation values after the knee and $\mu_{line}$ means the linear regime charge mobility. The mobility changes with $V_G$ are shown in Fig. S6b and d (online) for *f*-OTFTs using AgNWs and AgNWs-PEDOT:PSS as the gate electrode, respectively. The results suggest that the device mobilities should be corrected. Thus, the correction factor *r* is introduced to the calculation for obtaining more reliable mobility values. Using the average correction factor *r*, 32.9 and 33.6 $cm^2/(V\ s)$ are corrected to be 17.6 $cm^2/(V\ s)$ ($r$ = 53.4%) and 18.3 $cm^2/(V\ s)$ ($r$ = 54.5%), respectively.

Normally, indium tin oxide (ITO) deposited on PET substrate is used as the gate electrode in *f*-OTFTs. However, ITO is not the best choice since it is a ceramic material with high rigidity. The ITO gate electrode would crack under the small bending radius and cause damage to the device. The scanning electron microscope (SEM) images of devices fabricated on ITO/PET and bent at the radius of 6 mm are shown in Fig. S7 (online). It is very clear that ITO is cracked at 6 mm bending radius. The sheet resistances of ITO gate electrode before and after bending are compared in Fig. S8 (online). It is obvious that the sheet resistance of ITO/PET film rises nearly 20 times after bending, which would seriously affect the device performance. The mechanical bending characteristics of C8-BTBT *f*-OTFTs on AgNWs/PET and AgNWs-PEDOT:PSS/PET are measured at a bending radius of 6 mm, in which C8-BTBT *f*-OTFTs are bent perpendicular to the direction of source-drain current flow (Fig. S9 online). The typical transfer characteristic curves of C8-BTBT *f*-OTFTs using AgNWs and AgNWs-PEDOT:PSS gate electrodes before and after bending test with 2000 cycles are shown in Fig. S10a and b (online), and the statistical results of 20 devices are shown in Fig. 1e and f. As shown in Fig. S10a (online), the calculated mobilities for the same *f*-OTFTs before and after bending are 19.3 and 16.9 $cm^2/(V\ s)$, respectively. The *f*-OTFTs bent at a radius of 6 mm show a minor increase in off-current and an insignificant decrease in saturation current. Moreover, the $I_{on}/I_{off}$ ratio and $V_{th}$ exhibit little change. The statistical results indicate that the average mobility of C8-BTBT *f*-OTFTs with AgNWs decreases from 18.8 to 15.7 $cm^2/(V\ s)$ after a 2000 cycle bending test, about 17% degradation. In addition, Fig. S10b (online) shows that the mobility of a typical device before and after bending changes from 33.5 to 28.7 $cm^2/(V\ s)$ for *f*-OTFTs with AgNWs-PEDOT:PSS as the gate electrode. In comparison with *f*-OTFTs using AgNWs gate electrode, the average mobility of devices with AgNWs-PEDOT:PSS gate electrode is enhanced from 18.8 to 24.3 $cm^2/(V\ s)$. After the bending test, the average mobility still remains around 20.4 $cm^2/(V\ s)$. The $I_{on}/I_{off}$ ratio and $V_{th}$ are similar to the devices with AgNWs gate electrodes. Furthermore, all these mobilites are corrected via introducing the correction factor *r*, as shown in Table S1 (online). The corrected average mobilities are 10.0 and 8.0 $cm^2/(V\ s)$ for *f*-OTFTs with AgNWs gate electrode before and after bending, while the corrected average values are 13.2 and 10.6 $cm^2/(V\ s)$ for *f*-OTFTs with AgNWs-PEDOT:PSS gate electrode before and after bending. The average mobilities of both *f*-OTFTs decrease about 20% after bending 2000 cycles at a radius of 6 mm.

The PVP-HDA itself is a polar polymer due to its hydroxyl group, with dielectric constant of ~4.1 [18]. The low dielectric constant diminishes dielectric performance, with a high channel current leakage density in the range from about $3.6 \times 10^{-5}$ to $2.0 \times 10^{-4}$ $A/cm^2$. Fig. S11a and b (online) shows the evolution of leakage current density before and after 2000 cycles of bending. The statistical results show the average leakage current density of *f*-OTFTs with AgNWs gate electrode increases from $8.81 \times 10^{-5}$ to $1.53 \times 10^{-4}$ $A/cm^2$, and the average value of *f*-OTFTs with AgNWs-PEDOT:PSS gate electrode increases from $8.53 \times 10^{-5}$ to $1.42 \times 10^{-4}$ $A/cm^2$. Judging from the results, the dielectric property of cross-linked PVP-HDA on AgNWs or AgNWs-PEDOT:PSS gate electrode is comparable to previous findings [19]. The statistical results suggest that the solution-processed C8-BTBT *f*-OTFTs show good repeatability and high reliability. The increase of the leakage current density after bending is likely due to the mechanical distortion of thin-film morphology, which affects charge transport in the channel region. The atomic force microscope (AFM) morphology images of bent thin films are shown in Fig. S12 (online), and the root-mean-square (RMS) roughness values of PVP-HDA dielectric films increase from 2.36 to 5.87 nm.

The SEM images of C8-BTBT:PS thin films before and after bending are shown in Fig. S13 (online). The results suggest that the C8-BTBT:PS thin films exhibit good flexibility and stable morphology after bending. The structure of C8-BTBT:PS thin films on both gate materials before and after bending test is characterized via grazing incidence X-ray diffraction (GIXRD) and shown in Fig. S14a (online). The C8-BTBT thin film can be indexed via monoclinic phase with space group $P2_1/a$ [20], demonstrating a layer-by-layer structure with the molecular long axes aligned roughly perpendicular to the BTBT layer and BTBT moieties forming herringbone-packed monomolecular layers. The C8-BTBT molecules assembled in a π-conjugated herringbone manner and PS provided favorable nucleation dynamics for the crystal growth of C8-BTBT molecules. The long-range-ordered crystalline arrangement does not only facilitate charge transport, but also significantly reduces the channel resistance across the crystal film. It has been universally considered that charge transport is effectively driven by the first molecular layers close to the dielectric film in the case of OTFTs [21]. The layer-by-layer growth of C8-BTBT indicates a dense and continuous interface between gate dielectric and active channel, thus allowing very high mobility in the same direction [22]. Moreover, long-range order and low interlayer resistance are helpful to carrier transport as well [23]. The peak intensity of C8-BTBT:PS thin films before and after bending are shown in Fig. S14b (online). The results suggest the C8-BTBT thin films before and after bending exhibit strong diffraction peak with the similar intensity, indicating that the bending has no discernible influence on C8-BTBT thin film.

The above results suggest that the electrical properties of *f*-OTFTs are influenced by the gate electrodes. Generally, charge is always present in the non-ideal insulation layer of metal-insulator-semiconductor (MIS) structure. Due to these charges, an electric field is generated within the semiconductor's space charge layer, causing the semiconductor's energy band to curve away from the flat band state. Therefore, it is necessary to apply bias voltage to the gate electrode in order to counteract the semiconductor's band bending caused by the internal electric field. The different gate electrodes would result in various charge densities, affecting gate bias voltage and $V_{th}$ of *f*-OTFTs [24]. It was demonstrated that PVP is a hygroscopic material and can absorb water

to cause ionic species moving [25], which can increase the charge density at the interface between C8-BTBT and PVP-HDA, resulting in improving the device performance. Meanwhile, PVP as a hydroxyl-rich material could absorb water and cause surface polarization, leading to the higher saturation current [26]. The cross-linked PVP-HDA has abundant hydroxy function groups and the PEDOT:PSS is an aqueous solution exhibiting the water absorption effect. Therefore, the *f*-OTFTs with AgNWs-PEDOT:PSS gate electrode definitely have hygroscopic properties. The absorbed water changes the dielectric constant of the PVP-HDA layer and the charge trapping at the interface can occur, resulting in the devices with lower $V_{th}$ and higher mobility. The $V_{th}$ statistics of *f*-OTFTs on both gate electrodes are shown in Fig. S15 (online). It can be seen that the *f*-OTFTs with AgNWs-PEDOT:PSS exhibit lower $V_{th}$ values overall. The average $V_{th}$s are −2.8 and −3.3 V for *f*-OTFTs with AgNWs-PEDOT:PSS and AgNWs gate electrodes, respectively.

In summary, we fabricated *f*-OTFTs on a plastic PET substrate by using R2R slot-die coated AgNWs as the gate electrode, with the corrected highest and average mobilities up to 18.3 and 13.2 $cm^2/(V\ s)$, respectively. The superb compatibility of PET substrate, electrode materials, semiconductor layer and insulating film make *f*-OTFTs rival over rigid ones. Although the performance of *f*-OTFTs slightly degrades after 2000 successive bending cycles due to cumulative damage from external forces, *f*-OTFTs still show good performance parameters. As demonstrated above, our *f*-OTFTs have many advantages, such as high-mobility, excellent mechanical flexibility, low-cost, and straightforward reproducibility. The developments of manufacturing technology and organic materials such as these are expected to greatly advance the use of flexible electronics in daily life.

## Conflict of interest

The authors declare that they have no conflict of interest.

## Acknowledgments

This work was supported by the National Key Research and Development Program of China (2017YFA0206600) and the National Natural Science Foundation of China (51673214). Junliang Yang also thanks the support by State Key Laboratory of Powder Metallurgy at the Central South University.

## Author contributions

Pengshan Xie, Tianjiao Liu, and Jia Sun performed the experiments. Pengshan Xie, Tianjiao Liu, Jia Sun, and Junliang Yang prepared the manuscript. Pengshan Xie, Jia Sun, Jie Jiang, Yongbo Yuan, Yongli Gao, Jianfei Zhou and Junliang Yang participated in the discussion on experimental results. Junliang Yang directed this project.

## Appendix A. Supplementary materials

Supplementary materials to this article can be found online at https://doi.org/10.1016/j.scib.2020.03.013.

## References

[1] Tsumura A, Koezuka H, Ando T. Macromolecular electronic device: field-effect transistor with a polythiophene thin film. Appl Phys Lett 1986;49:1210–2.
[2] Sirringhaus H. 25th anniversary article: organic field-effect transistors: the path beyond amorphous silicon. Adv Mater 2014;26:1319–35.
[3] Diao Y, Shaw L, Bao Z, et al. Morphology control strategies for solution-processed organic semiconductor thin films. Energy Environ Sci 2014;7:2145–59.
[4] Yang J, Yan D, Jones TS. Molecular template growth and its applications in organic electronics and optoelectronics. Chem Rev 2015;115:5570–603.
[5] Schwartz G, Tee BCK, Mei J, et al. Flexible polymer transistors with high pressure sensitivity for application in electronic skin and health monitoring. Nat Commun 2013;4:1859.
[6] Jiang C, Choi HW, Cheng X, et al. Printed subthreshold organic transistors operating at high gain and ultralow power. Science 2019;363:719.
[7] Chen Y, Au J, Kazlas P, et al. Flexible active-matrix electronic ink display. Nature 2003;423:136–136.
[8] Fu Y, Kong L, Chen Y, et al. Flexible neuromorphic architectures based on self-supported multiterminal organic transistors. ACS Appl Mater Interfaces 2018;10:26443–50.
[9] Ji D, Li T, Zou Y, et al. Copolymer dielectrics with balanced chain-packing density and surface polarity for high-performance flexible organic electronics. Nat Commun 2018;9:2339.
[10] Wang S, Xu J, Wang W, et al. Skin electronics from scalable fabrication of an intrinsically stretchable transistor array. Nature 2018;555:83–8.
[11] Wang Q, Jiang S, Qiu L, et al. Interfacial flat-lying molecular monolayers for performance enhancement in organic field-effect transistors. ACS Appl Mater Interfaces 2018;10:22513–9.
[12] Yuan Y, Giri G, Ayzner AL, et al. Ultra-high mobility transparent organic thin film transistors grown by an off-centre spin-coating method. Nat Commun 2014;5:3005.
[13] Duan S, Gao X, Wang Y, et al. Scalable fabrication of highly crystalline organic semiconductor thin film by channel-restricted screen printing toward the low-cost fabrication of high-performance transistor arrays. Adv Mater 2019;31:1807975.
[14] Ren H, Cui N, Tang Q, et al. High-performance, ultrathin, ultraflexible organic thin-film transistor array via solution process. Small 2018;14:1801020.
[15] Tong S, Sun J, Yang J. Printed thin film transistors: research from China. ACS Appl Mater Interfaces 2018;10:25902.
[16] Choi HH, Cho K, Frisbie CD, et al. Critical assessment of charge mobility extraction in FETs. Nat Mater 2018;17:2–7.
[17] Bittle EG, Basham JI, Jackson TN, et al. Mobility overestimation due to gated contacts in organic field-effect transistors. Nat Commun 2016;7:10908.
[18] Roberts ME, Queraltó N, Mannsfeld SCB, et al. Cross-linked polymer gate dielectric films for low-voltage organic transistors. Chem Mater 2009;21:2292–9.
[19] Huang Y, Sun J, Zhang J, et al. Controllable thin-film morphology and structure for 2,7-dioctyl[1]benzothieno[3,2-b][1]benzothiophene (C8BTBT) based organic field-effect transistors. Org Electron 2016;36:73–81.
[20] Izawa T, Miyazaki E, Takimiya K. Molecular ordering of high-performance soluble molecular semiconductors and re-evaluation of their field-effect transistor characteristics. Adv Mater 2008;20:3388–92.
[21] Zhang H, Guo X, Hui J, et al. Interface engineering of semiconductor/dielectric heterojunctions toward functional organic thin-film transistors. Nano Lett 2011;11:4939–46.
[22] He D, Qiao J, Zhang L, et al. Ultrahigh mobility and efficient charge injection in monolayer organic thin-film transistors on boron nitride. Sci Adv 2017;3:1701186.
[23] Kwon S, Kim J, Kim G, et al. Organic single-crystal semiconductor films on a millimeter domain scale. Adv Mater 2015;27:6870–7.
[24] Grove A. Physics and technology of semiconductor devices. New York, NY: Wiley; 1967. p. 366.
[25] Bäcklund TG, Sandberg HGO, Österbacka R, et al. Current modulation of a hygroscopic insulator organic field-effect transistor. Appl Phys Lett 2004;85:3887–9.
[26] Jung T, Dodabalapur A, Wenz R, et al. Moisture induced surface polarization in a poly(4-vinyl phenol) dielectric in an organic thin-film transistor. Appl Phys Lett 2005;87:182109.

Pengshan Xie received the B.S. degree from Central South University in 2017. Currently, he is a graduate student at Central South University, China. His research interests are focused on the functional layers of high-performance organic thin-film transistors.

Tianjiao Liu received the B.S. degree from Hunan Normal University in 2016. She received the master's degree from Central South University in 2019. Her research interest is high-performance organic thin-film transistors.

Jia Sun received his Ph.D. degree from Hunan University in 2012. He was a postdoctoral researcher in Central South University (2012–2014) and Sungkyunkwan University (2017–2018). In 2014, he joined the faculty at Central South University and is currently a professor in Scholl of Physics and Electronics. His research interests focus on novel photoelectronic devices and neuromorphic devices.

Junliang Yang received his Ph.D. degree in 2008 from Changchun Institute of Applied Chemistry, Chinese Academy of Sciences. He then joined Prof. Tim S. Jones' group at the University of Warwick. In April 2011, he moved to Australia and joined Prof. Andrew B. Holmes' group at the University of Melbourne and at the Commonwealth Scientific and Industrial Research Organisation. In 2012, he was appointed as a professor in the School of Physics and Electronics at Central South University. His research focuses on flexible and printed electronics, organic and perovskite solar cells.